RESEARCH ARTICLE | OCTOBER 27 2022

Biphasic flow dynamics and polarized mass transportation in branched hepatic sinusoids

Yinjing Hao; Shouqin Lü; Wang Li; ... et. al

Biomicrofluidics 16, 054110 (2022)
https://doi.org/10.1063/5.0100911

Biomicrofluidics ARTICLE scitation.org/journal/bmf

Biphasic flow dynamics and polarized mass transportation in branched hepatic sinusoids

Cite as: Biomicrofluidics **16**, 054110 (2022); doi: 10.1063/5.0100911
Submitted: 27 May 2022 · Accepted: 28 September 2022 ·
Published Online: 27 October 2022

Yinjing Hao,[1] Shouqin Lü,[2,3] Wang Li,[2,3] Mian Long,[2,3,a)] and Yuhong Cui[1,a)]

AFFILIATIONS

[1]Department of Mechanics, Tianjin University, Tianjin 300072, China
[2]Center of Biomechanics and Bioengineering, Key Laboratory of Microgravity (National Microgravity Laboratory), Beijing Key Laboratory of Engineered Construction and Mechanobiology, Institute of Mechanics, Chinese Academy of Sciences, Beijing, China
[3]School of Engineering Science, University of Chinese Academy of Sciences, Beijing, China

[a)]**Authors to whom correspondence should be addressed:** mlong@imech.ac.cn, **Tel.:** +86 10 8254 4131, **Fax:** +86 10 8254 4131 and yhcui@tju.edu.cn, **Tel.:** +86 22 27404934, **Fax:** +86 22 27404934

ABSTRACT

In fatty liver diseases, such as liver fibrosis and liver cirrhosis, blood flow in hepatic sinusoids, an elementary building block of the liver lobule, tends to bypass through collateral vessels inside sinusoids and presents distinct sinusoidal flows compared to normal physiological flows. It remains unclear in those flow characteristics in branched sinusoids and the correlation of pathological flows with liver lesions, mainly due to the difficulty of direct hemodynamics measurements in the sinusoids. Here, we developed a dual-branched theoretical model of hepatic sinusoidal flow to elucidate the relevant flow dynamics and mass transport. Numerical simulations, based on the lattice Boltzmann method, indicated that the flow velocity distribution in hepatic sinusoids is mainly dominated by endothelium permeability and presents a non-monotonic variation with the permeability at the fusion segment of these branched sinusoids. Flow-induced shear stress on the endothelium at the side of the Disse space exhibited a biphasic pattern, yielding a low shear stress region at the junctional site. Meanwhile, a highly polarized distribution of lipoproteins concentration was also presented at the low shear stress region, indicating a localized accumulation of typical hepatic serum proteins. Thus, this work provides the basic understanding of blood flow features and mass transport regulations in branched hepatic sinusoids.

INTRODUCTION

The liver is an important organ that plays a critical role in protein synthesis and toxin metabolism, which is also susceptible to various diseases.[1,2] Experimental and numerical studies indicate that liver lesions are usually accompanied by hemodynamic changes, resulting in the abnormal blood flow characteristics in the Disse space that is different from the normal physiological environment,[3–8] especially in liver fibrosis and cirrhosis, as the basic unit of hepatic blood flow, pathological hepatic sinusoids undergo the structural remodeling,[9,10] leading to remarkable variations of the hepatic sinusoids tortuosity and the formation of bypass vessels, which yields irregular geometries of hepatic sinusoids with numerous branched structures.[5,11] Those branched structures can significantly alter the blood flow characteristics in hepatic sinusoids. Therefore, the hepatic sinusoid blood flow is closely related to the liver diseases and understanding the flow characteristics in branched hepatic sinusoids is of great importance to elaborate the hemodynamics changes in such diseases as liver fibrosis and cirrhosis.

Except for other factors that affect hepatic lipid metabolisms, such as alcoholic effects,[12] thyroid hormones,[13] endoplasmic reticulum (ER) stress,[14,15] and insulin signaling,[16] blood flow characteristics are also related to the hepatic lipid metabolism, especially to the accumulation of triglycerides (TGs) in hepatocytes, which is associated with the lipid metabolism.[17] The sources of intracellular TGs in hepatocytes are as follows: free fatty acids (FFAs) released from adipose tissue to the peripheral circulation are absorbed and esterified to produce TGs.[18] In

glycolipid conversion, acetyl coA, the oxidation product of glucose, is used as raw material to synthesize de novo fatty acids, which are esterified to produce TGs. Under normal physiological conditions, the esterification of peripheral circulating fatty acids into TGs is predominated in hepatocytes. The uptake of FFA and in turn the formation of TGs are related to the degree of effective hepatic blood flow.[19] Impaired blood flow caused by increased intrahepatic vascular resistance induces local tissue hypoxia, which subsequently triggers several pathways that ultimately lead to the progression of non-alcoholic fatty liver disease (NAFLD) to non-alcoholic steatohepatitis (NASH) and its further hepatic and extrahepatic complications as well as intrahepatic TG formation.[20] Therefore, hepatic sinusoidal blood flow characteristics are closely related to both branched structures in hepatic diseases and hepatic lipid metabolism.

Existing experimental techniques are able to visualize hepatic sinusoid blood flow, but still with many limitations.[7,21] For example, Doppler ultrasound imaging,[22,23] *in vivo* two-photon confocal imaging,[24,25] and transmission electron microscopy,[26] often used to illustrate the hepatic flows and structures, cannot measure parameters such as blood velocity and pressure difference in hepatic sinusoids. Numerical simulations can serve as a prevalent method for elucidating hepatic sinusoidal blood flow and mass transport. For instance, hepatic sinusoidal blood flow is predicted numerically by considering the effects of endothelial sieve pores but not refined structures, such as the Disse space.[27] Impacts of blood flow on serum ammonia metabolism in hepatocytes are analyzed in a microchannel that does not contain a porous permeable membrane.[28] In addition, inflammatory response to *Salmonella* is tested in hepatic sinusoids even without considering the contribution of blood flow.[29] Nevertheless, the blood flow characteristics of a hepatic sinusoid in the branched structure under the environment of liver diseases and the effect of blood flow on hepatic sinusoid mass transport are much less understood. Therefore, quantifying the effects of these branched structures on the blood flow characteristics and the blood flow characteristics effects on hepatic mass transport are required.

Previously, we analyzed the flow dynamics in pathophysiological liver lobules with branched vessels[11] and also the blood flow characteristics in a long straight sinusoid with varied endothelial permeability.[30] Here, flow-induced shear stress and mass transfer profiles for the bifurcated hepatic sinusoids were elucidated using a typical dual-branched model. This issue initially comes from the fact that the bypassed blood circuits are often formed to maintain the required blood supply inside the fibrotic or cirrhotic liver. The physical problem behind this pathophysiological feature is how to elucidate the effects of this bifurcation structure of the branched hepatic sinusoids on the flow dynamics characteristics and mass transport features, as compared to those of straight sinusoids. Therefore, it is crucial to understand the hemodynamics in a bifurcated hepatic sinusoid on liver diseases. In this work, a body of flow and transport parameters were obtained numerically, including blood flow velocity in hepatic sinusoids with a branched structure; flow-induced shear stress on the endothelial surface; and effects of different endothelial permeabilities on fatty acid transportation, fatty acid and glyceride metabolism, and low-density lipoprotein deposit in hepatic sinusoids. Additionally, we further analyzed those specialized effects of the bifurcated structures on how hepatic sinusoidal blood flow regulates physiological functions under complicated pathological conditions.

MATERIALS AND METHODS

Governing equations for blood flow in a dual-branched hepatic sinusoidal model

The Disse space is present between hepatocytes and endothelium and filled with collagen matrices in the fibrotic liver. Collagen deposits onto the hepatocyte surface and affects interstitial flow together with the existence of hepatocyte villi. The endothelium divides a hepatic sinusoid into three regions of sinusoidal cavity, endothelial cell layer, and Disse space. A simplified model of a dual-branched hepatic sinusoid was developed with two branched inlets and outlets, as given geometries shown in Fig. 1(a). Here, the blood flows in from the inlets of the two left branches, converges in the middle segment, and then flows out from the outlets of the two right branches.

A lattice Boltzmann method (LBM) was applied [Fig. 1(b)], which is derived from microscale low-speed flows and suitable for fluid–structure coupling calculations with multiple interfaces.[30] Based on the original lattice Boltzmann equation, the effects of the endothelium and hepatocyte microvillus and collagen layer on blood flow were tested by introducing two additional force terms of P_i and R_i into the governing equation. The governing equations are expressed in dimensionless lattice units, as follows:[30]

$$g_i(\mathbf{x}+\mathbf{v_i}\Delta t, t+\Delta t) - g_i(\mathbf{x}, t) = -[g_i(\mathbf{x}, t) - g_i^{eq}(\mathbf{x}, t)]/\tau + \Delta t \cdot P_i + \Delta t \cdot R_i \ (i = 0, 1, 2, 3, \ldots, 8), \quad (1)$$

where g_i is the distribution function for a particle with velocity $\mathbf{v_i}$ at position $\mathbf{x}$ at time t; $\mathbf{v_i}$ is the distribution function of the migration distance along the ith direction per unit time, i.e., the migration velocity; g_i^{eq} is the equilibrium distribution function; and Δt is the time increment. τ is the dimensionless relaxation time associated with blood viscosity. Two external force terms, P_i and R_i, were introduced to account for the extra effects of the endothelial layer and the hepatic villi and collagen layer (HMVCL) on the flow, respectively.[30] The endothelial layer was assumed to be a porous media layer and the flow in the layer satisfies Darcy's law. The hepatic villi and collagen layer (HMVCL) were assumed as porous media layers with uniform thickness to unify the effects of surface roughness on the flow. The descriptions of the two external force terms can be referred in the previous publication.[30] Of note, the continuity of pressure and velocity was also satisfied on the interfaces between endothelial layer and sinusoid cavity and the interfaces between HMVCL and the Disse space. Those two external source terms were assumed to be zero outside the regions of the endothelium and HMVCL.

After obtaining the distribution function g_i ($\mathbf{x}$, t) from Eq. (1), we can determine those physical quantities, density ρ, velocity $\mathbf{u}$, and pressure p, of the blood flow. The corresponding calculating

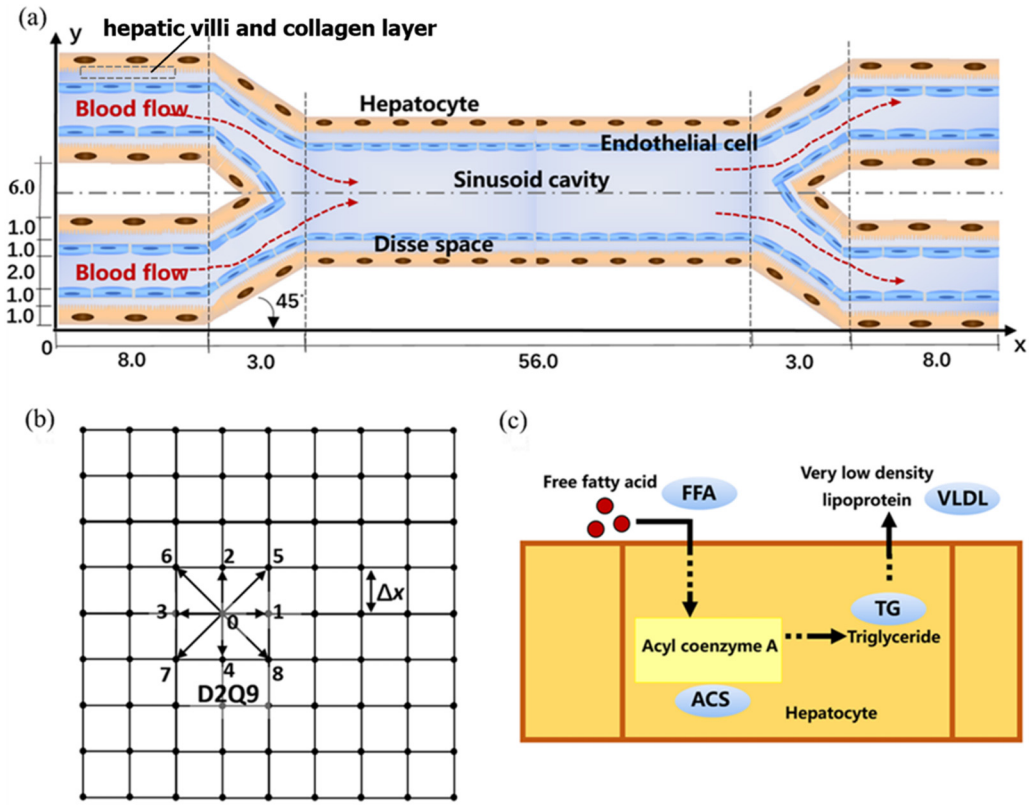

FIG. 1. (a) Schematic model of a dual-branched hepatic sinusoid (unit: μm). (b) A numerical D2Q9 model based on the lattice Boltzmann numerical method. (c) Schematic of hepatocytes metabolism of free fatty acids (FFAs) to produce triglycerides (TGs) and convert TGs to very low-density lipoprotein (VLDL) for transport outside the hepatocytes.

equations are the same as Eqs. (14a)–(14c) with identical simulating algorithms of LBM introduced in Ref. 30.

Governing equations for mass transport in a dual-branched sinusoidal model

Lipid deposition is a key biochemical event in initiating and aggravating fatty liver diseases, which is also associated with flow dynamics inside the sinusoidal cavity and the Disse space. To mimic this flow-accompanied mass transport, the process for FFAs intake and TG production was simplified as FFA consumption and VLDL/TG production, as shown in Fig. 1(c). The LBM was again applied to calculate their convection and diffusion of FFA and VLDL. The LBM method is used to solve the equations, mainly considering the micro-flow characteristics on the low Rayleigh number at the micro-scale, which is more accurate when the scale is within the range of 0.1–1 μm[5] as compared to those from the Finite-difference method. Furthermore, the low Reynolds number caused by the small sizes of sinusoidal lumen and space of Disse is also critical in deciphering the related fluid field experimentally. Thus, this work established a liver sinusoidal model using the LBM method, attempting to numerically explore the blood flow characteristics of low Reynolds number and micro-sized liver sinusoids. The governing equations are as follows:

$$g_i(\mathbf{x}+\mathbf{v}_i\Delta t,\, t+\Delta t) - g_i(\mathbf{x},\, t) = -[g_i(\mathbf{x},\, t) - g_i^{eq}(\mathbf{x},\, t)]/\tau_{FFA} + \Delta t\omega_i S_{FFA}\ (i = 0,\, 1,\, 2,\, 3,\, \ldots,\, 8), \tag{2}$$

$$g_i(\mathbf{x} + \mathbf{v_i}\Delta t,\, t + \Delta t) - g_i(\mathbf{x},\, t) = -[g_i(\mathbf{x},\, t) - g_i^{eq}(\mathbf{x},\, t)]/\tau_{VLDL} + \Delta t\omega_i S_{VLDL}\ (i = 0,\, 1,\, 2,\, 3,\, \ldots,\, 8), \tag{3}$$

$$g_i^{eq}(\mathbf{x},\, t) = \omega_i C(1 + \mathbf{v}_i \cdot \mathbf{u}/\mathbf{c}_s^2)\ (i = 0,\, 1,\, 2,\, 3,\, \ldots,\, 8), \tag{4}$$

where ω is the weight coefficient with the values of $\omega_0 = 4/9$, $\omega_i = 1/9$ ($i = 1$–4), $\omega_i = 1/36$ ($i = 5$–8); $\mathbf{x}$ represents the node position of flow field, τ is the dimensionless relaxation time, which is related to the diffusion coefficient, $\mathbf{u}$ is the flow fluid velocity, and $\mathbf{c}_s$ is the speed of sound. For a D2Q9 model, the migration velocity can be referred to in the literature.[30] The last term in Eqs. (2) and (3) denotes an

exogenous term in the convection–diffusion equation. The subscripts FFA and VLDL stand for free fatty acids and very low-density lipoprotein (VLDL), respectively. In this work, the mass transport is only assumed to satisfy the convective-diffusion equation. The reaction source terms $\Delta t\omega_i S_{FFA}$ and $\Delta t\omega_i S_{VLDL}$ in the convection–diffusion equations (2) and (3) represent, respectively, the metabolic consumption of sinusoidal free fatty acids and the conversion of intracellular fatty acids into lipoproteins by hepatocytes. The convective-diffusion equations used in the calculation of free fatty acids and lipoproteins are the same except for their different reaction source terms.

The relationships between mass concentrations, diffusion coefficients, and physical quantities are termed as follows:

$$D_{FFA} = \mathbf{c}_s^2(\tau_{FFA} - 0.5)\Delta t, \tag{5}$$

$$D_{VLDL} = \mathbf{c}_s^2(\tau_{VLDL} - 0.5)\Delta t, \tag{6}$$

$$C(\mathbf{x}, t) = \sum\nolimits_i g_i(\mathbf{x}, t), \tag{7}$$

$$C(\mathbf{x}, t) \cdot \mathbf{u}(\mathbf{x}, t) = \sum\nolimits_i g_i(\mathbf{x}, t)\mathbf{v}_i, \tag{8}$$

$$S_{FFA} = k_{FFA} C_{FFA}(\mathbf{x}, t), \tag{9}$$

$$S_{VLDL} = k_{VLDV} C_{FFA}(\mathbf{x}, t), \tag{10}$$

where C is the mass concentration, D_{FFA} and D_{VLDL} denote the diffusion coefficients of respective FFAs and VLDLs, and $\mathbf{u}$ is the flow field velocity, which is derived from the stable solution of the flow velocity in the above flow field calculation and then directly input here. $k_{FFA}C_{FFA}$ in Eq. (9) is an exogenous term for FFA consumption, in which k_{FFA} represents the reaction rate and yields a non-zero constant on the hepatocytes wall but zero in other regions of the sinusoid. $k_{VLDL}C_{FFA}$ in Eq. (10) serves as an exogenous term for VLDL production, in which k_{VLDL} represents the VLDL reaction rate with a non-zero value on the hepatocytes wall but with zero value in other regions under similar FFA concentration C_{FFA}, suggesting that, when the concentration of fatty acids C_{FFA} is zero, this item is zero and, thus, no TG and VLDL is produced. FFA and VLDL concentration distributions were obtained by solving Eqs. (2) and (3).

TABLE I. Relevant parameters used in the calculation.

Parameter	Values
Density ρ	1000 kg m^{-3}
Kinematic viscosity μ	1.2 cp[32]
Re	0.0012
Dimensionless relaxation time τ	1.1
Permeability coefficient of endothelial layer k	10^{-16}–10^{-13} m^2 (estimated by Ref. 33)
Permeability coefficient of hepatic villi and collagen layer k_r	10^{-16}–10^{-14} m^2 (estimated by Ref. 32)

Numerical calculations for flow field and mass transport

The configuration and geometry of the calculating model are shown in Fig. 1(a). The size of the actual computational domain is $12.0 \times 80.0\,\mu$m^2, corresponding to a total of 120×800 grids in numerical calculation. No slip boundary condition is assumed on the hepatocyte surface. The inlet flow rate is set to be 8.14×10^{-5} ml min^{-1}, with an inlet Reynolds number (*Re*) of 0.0012. The outlet is free to flow out, with the velocity settings as that y-velocity is zero and x-velocity adopts the mass-modified outlet boundary condition to ensure flow conservation. The plasma is assumed to be an incompressible Newtonian fluid with a viscosity of 1.2 cp and a density of 1000 kg m^{-3}. A dimensionless relaxation time $\Delta t/\tau$ was used in LBM equations and our programming codes, and the relaxation time in LBM is related to the value of fluid viscosity coefficient μ_D. The computational stability and accuracy of the model used in this work have been validated in our previous work[30] and other studies.[5] The permeability coefficient, k, of the endothelial layer is ranged at 10^{-16} m^2–10^{-13} m.[29] The hydraulic resistivity of the macromolecular layer adjacent to the endothelium is assigned to be a value of $\sim 10^8$ dyn s cm^{-4} in the literature,[31] from which the endothelial permeability coefficient is estimated to be approximately 10^{-14} m^2. Thus, the permeability coefficient of the hepatic microvilli and collagen layer, k_r, is set on a scale between 10^{-16} and 10^{-14} m^2. The higher the permeability coefficient, the greater is the porosity of the hepatocyte villi and collagen layer, indicating relatively sparse collagen filling. All calculated parameters were summarized in Table I. The convergence criterion for the steady state of the flow was given for the relative error of velocity of less than 10^{-6}.[5,30] Total 1.0×10^4–2.0×10^4 time steps were set for calculating blood flow, yielding a physical duration of 1–3h when the calculation time step is 1.67×10^{-8} s. By selecting different grid number sets of 60×400, 120×800, and 180×1200, it was found that this 120×800 set evidently meets both the requirements of computational accuracy and efficiency (*data not shown*).

The boundary conditions for mass transport calculation are set as follows: FFA concentrations at sinusoidal inlet and outlet are $C_{FFA} = C_0$ and $\partial C_{FFA}/\partial x = 0$, respectively. Inlet and outlet TG concentrations are set as periodic boundary conditions. The diffusion coefficients and parameters of FFA and VLDL are summarized in Table II. The codes were programmed using Fortran language. The computational accuracy and reliability were verified by Poiseuille pressure-driven flow, resulting in an error within 1% between analytical solution and numerical estimation.

TABLE II. Parameters of convection–diffusion calculation.

Parameter	Values
Inlet concentration C_0	6.0×10^{-6} mol m^{-3}
FFA diffusion coefficient D_{FFA}	2.0×10^{-11} m^2 s^{-1}[24,34]
VLDL diffusion coefficient D_{VLDL}	2.0×10^{-11} m^2 s^{-1}[24,34]
FFA metabolic rate k_{FFA}	3.0×10^3 s^{-1}
VLDL production rate k_{VLDL}	3.0×10^3 s^{-1}

RESULTS

Flow velocity profiles inside sinusoidal cavity

We first tested the effect of different endothelial permeability on the flow velocity in a branched sinusoid. A typical velocity distribution of sinusoidal flow at an endodermal permeability coefficient of $10^{-16}\,m^2$ is shown in Fig. 2(a) and the flow velocity profiles at the middle cross section of the confluence segment are illustrated in Fig. 2(b). Results indicated that maximum velocity in the sinusoidal cavity decreases and maximum velocity in Disse space increases with increasing endothelial permeability when the endothelial permeability $k > 10^{-15}\,m^2$. In contrast, maximum velocity in sinusoidal cavity decreases and maximum velocity in Disse space increases with decreasing permeability when $k < 10^{-15}\,m^2$, presenting a non-monotonic transition of flow velocity at the confluence sinusoid with endothelial permeability. Compared with those in a straight sinusoid (*solid lines*; also referring the literature[30]), the flow velocity was higher when $k < 10^{-5}\,m^2$ but not significantly different when $k > 10^{-15}\,m^2$ in a branched sinusoid (*dotted lines*).

To elucidate the underlying regulations of this non-monotonic transition manner, the confluence segment of the sinusoidal cavity was zoomed in and segregated into the three sections of the branching subsection (Q_1), the inner Disse space subsection 1 (Q_2), and the outer Disse space subsection 2 (Q_3) [Fig. 2(c)]. Evidently, the smaller the endothelial permeability coefficient, the greater the flow in Q_1 and the less the flow in Q_2. Decrease in the flows inside the two Disse space subsections exceeds the flow increase in the branching subsection when $k \leq 10^{-15}\,m^2$, thus resulting in a decrease in the flow rate in the sinusoidal cavity. In the branching segment that is featured as the bifurcation fusion (*point* no. 8) and the re-bifurcation (*point* no. 9) [Fig. 1(a)], the flow velocity in the sinusoidal cavity in Q_1 decreases or in the Disse space in Q_3 increases, with increasing endothelial cells permeability (*dotted circles*) [Figs. 2(d) and 2(e)]. These results are consistent with the above non-monotonic transition manner for flow velocity with endothelial permeability after the branches are converged. In a single-straight sinusoid, however, the flow in the sinusoidal cavity does not contain Q_3, and the velocity only shows a monotonic transition with the endothelial permeability.[30] In addition, the flow velocity at the outlet re-bifurcation in the Disse space is slightly higher than that at the inlet bifurcation fusion (*dotted circles*) [Figs. 2(d) and 2(e)], presumably due to the outflow in the Disse space at the bifurcation fusion and the inflow in the Disse space at the re-bifurcation.

The average flow velocity at different cross sections of Disse space was further compared [Fig. 2(f)]. The blood flow velocity near the inner side of the branch segment (*points* no. 1 and no. 7) is much smaller than that near the outer side (*points* no. 2 and no. 6). In contrast, much smaller differences in flow velocity exist between these cross sections in the middle confluence segment (*points* no. 3, no. 4, and no. 5). Additionally, the velocity gradually decreases in the branch segment and gradually increases in the confluence segment when the endothelial permeability increases. Collectively, the flow velocity profile demonstrates a different transition pattern in a dual-branched sinusoid from a single-straight sinusoid, mainly due to the effects of the branched configuration, *that is*, a non-monotonic transition for the former and a monotonic transition for the latter in the sinusoidal cavity with varied endothelial permeability.

Shear stress profiles on hepatocytes and endothelium surface

Vast amount of collagen is deposited into Disse space during liver fibrosis or cirrhosis. When these collagen substances attach to the surface of hepatocytes, they form a rough wall layer together with hepatic microvilli, which affects the flow-induced shear stress in the Disse space. Here, we further tested the effects of the endothelial layer, hepatic microvilli, and collagen layer on shear stress exerted on the endothelial surface. Concerning the upper and lower surfaces of endothelial cells at the middle cross section of the confluence segment in the branched sinusoid ($x = 40\,\mu m$), the shear stress presents a biphasic pattern on the lower surface (facing to Disse space) [Figs. 3(b) and 3(d)] but not this visible transition on the upper surface (facing to the sinusoidal cavity) [Figs. 3(a) and 3(c)] with varied endothelial thicknesses and permeability coefficients. This transition pattern of shear stress is consistent with that for a single-straight sinusoid.[30] In addition, the shear stress is significantly different when varying endothelial and microvilli thicknesses showed in Figs. 3(a)–3(d). It shows a non-monotonic transition with varied endothelial permeability, *that is*, decreasing with increasing endothelial permeability when $k > 10^{-15}\,m^2$ but increasing with increasing endothelial permeability when $k < 10^{-15}\,m^2$ [Figs. 3(a)–3(d)], corresponding to the non-monotonic transition in flow velocity with endothelial permeability (Fig. 2), which is related to the velocity gradient. In contrast, the shear stress in the single-straight sinusoid varies monotonously with the endothelial permeability.[30]

In contrast to the single-straight sinusoid, the distribution of shear stress in the dual-branched sinusoid is not uniform, with evident regions of low shear stress at the branches. Concerning those endothelial cells located at the inner side of the branches in the range of $x = 67.0$–$77.0\,\mu m$, the shear stress on the upper surface of endothelial cells is the smallest and close to zero at the branching intersection point, i.e., $x = 67.0\,\mu m$, and is increased as x increases, away from the branching region [Figs. 3(e)–3(j)]. This indicates a low shear stress region existing near the branches, which is mainly distributed in the core cavity and at the branching intersection [Fig. 3(k)]. Shear stress exerted on the endothelium becomes smaller in the gentler distribution when the endothelial permeability coefficient is increased but is higher in the more uneven distribution when the permeability coefficient is decreased. This implies that, when the endothelial permeability decreases, the endothelial cells are subjected to higher shear stress with a sharp increase at the inflection point of the flow. Together, the shear stress in the dual-branched sinusoid also demonstrates a biphasic pattern compared with the single-straight sinusoid. Meanwhile, the stress presents a non-monotonic transition with an obvious region of low shear stress at the branching intersection.

FFA and vLDL transport

FFAs are usually forced to flow into the left entrance of the dual-branched sinusoid and subsequently consumed by hepatocytes

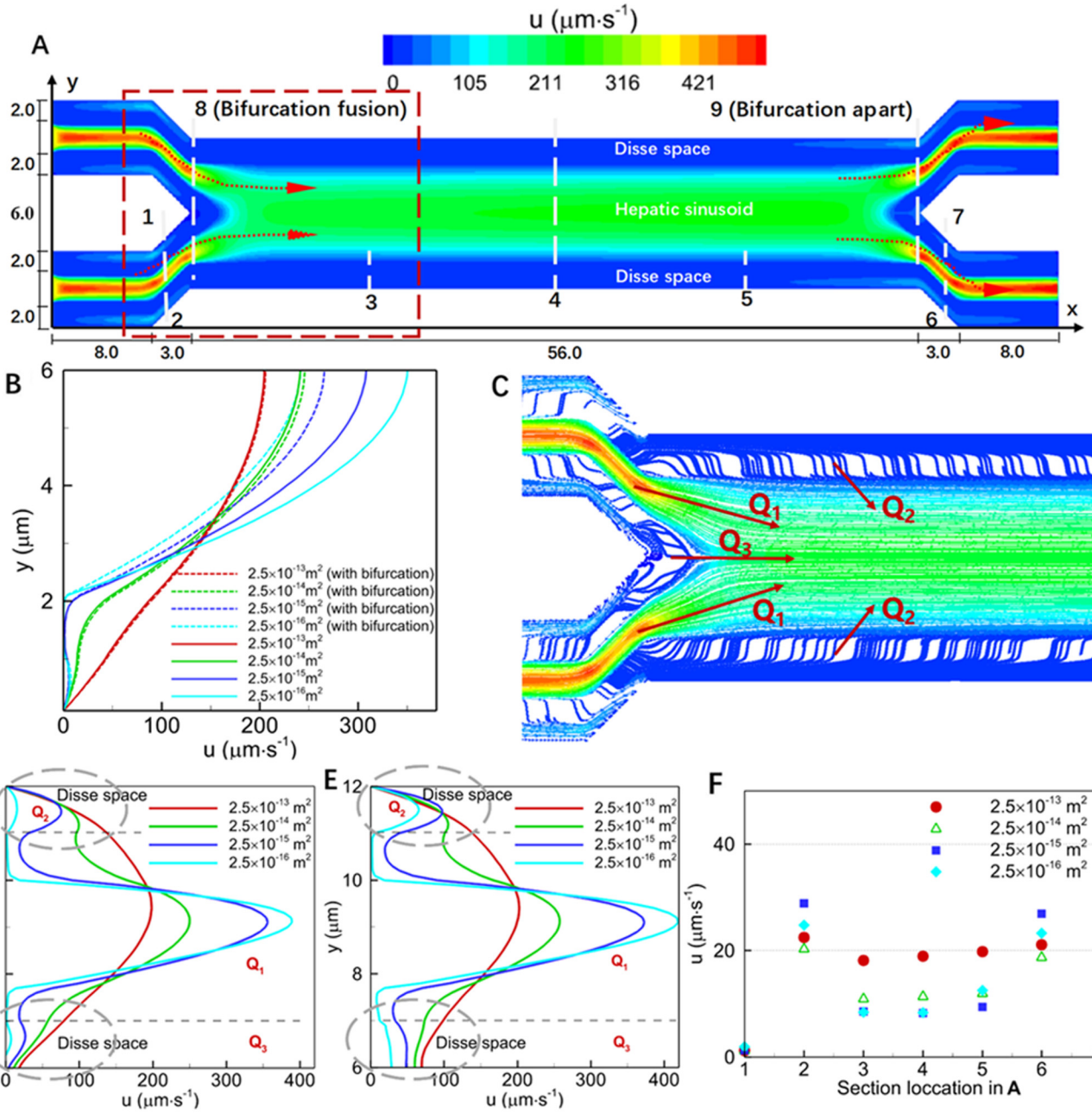

FIG. 2. (a) Flow velocity distribution in a branched sinusoid model at endothelial cell permeability of 2.5×10^{-16} m^2. (b) Comparison between a dual-branched sinusoid and a single-straight sinusoid on flow velocity profile at middle cross section indicated as a *dotted line of section no.* 4 in (a). (c) Enlarged flow velocity distribution in hepatic sinusoid branched model as depicted in a *dotted* box in (a). (d) and (e) Profiles of flow velocity at $x = 11.5\,\mu$m (bifurcation fusion section no. 8) (d) or $x = 68.5\,\mu$m (re-bifurcation section no. 9) (e). (f) Average velocity in Disse space at different cross section positions indicated in Fig. 1(a). no. 1, no. 2: $x = 9.0\,\mu$m; no. 3: $x = 25.0\,\mu$m; no. 4: $x = 40.0\,\mu$m; no. 5: $x = 55.0\,\mu$m; and no. 6, no. 7: $x = 71.0\,\mu$m.

at given reaction rates after entering Disse space through the endothelium. Figures 4(a)–4(d) show that the difference in FFA concentration with varied endothelial permeabilities is significant only at the entrance or exit branch but insignificant at those middle cross sections. Here, we calculate the differences in FFA concentration between different permeability coefficients and those of 2.5×10^{-16} m^2/s. For a double-branched sinusoid with the permeability coefficient decreasing from 2.5×10^{-13} to 10^{-16} m^2/s, the

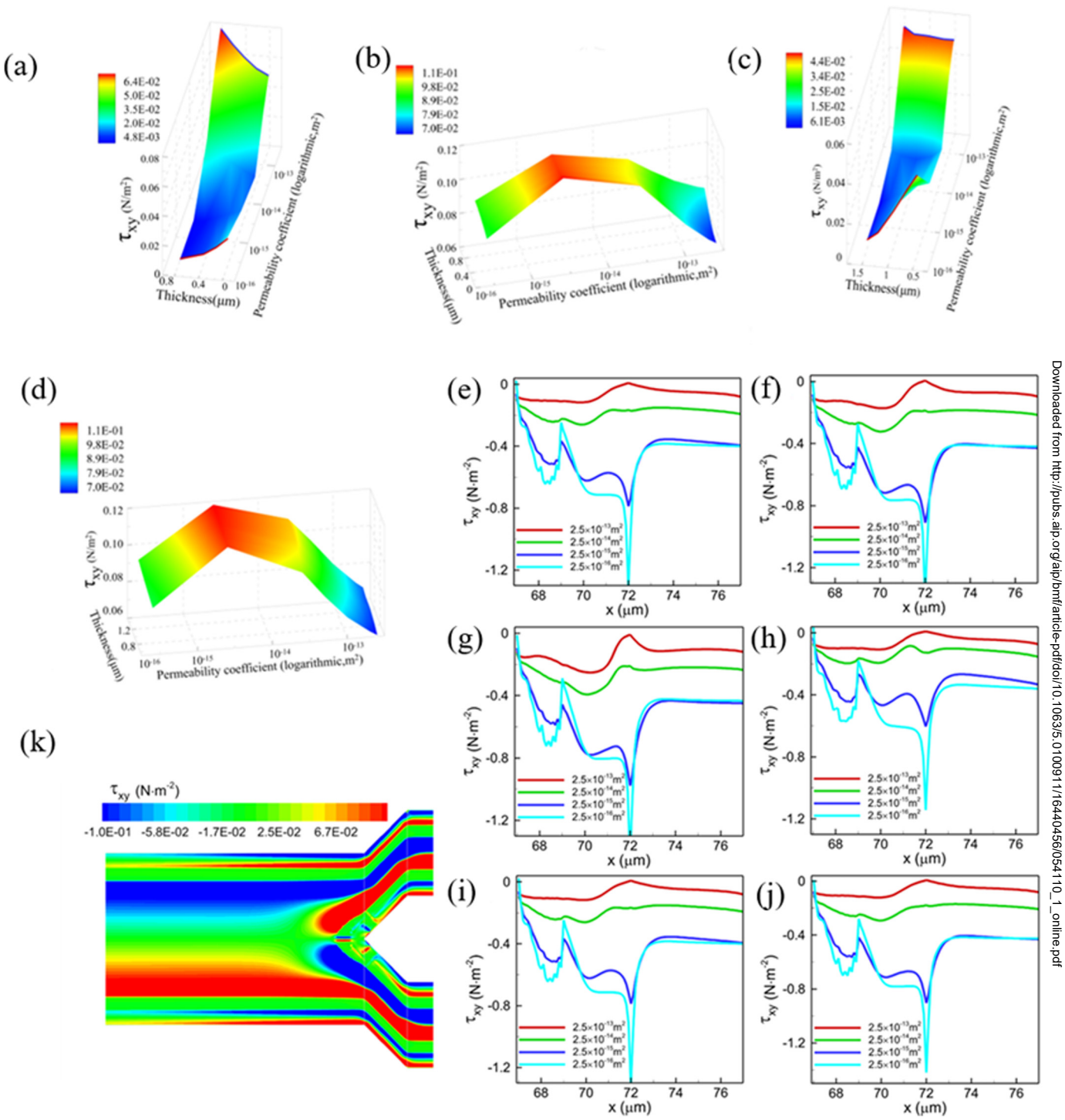

FIG. 3. (a)–(d) Shear stress profiles at the side of Disse space [(a) and (c)] or sinusoidal cavity [(b) and (d)] on endothelium under varied hepatic microvillus thicknesses [(a) and (b)] or endothelium thickness [(c) and (d)]. *Red* or *black lines* were added in *a* or *c* to visualize their trends explicitly. (e)–(j) Distribution of flow-induced shear stress along the intersection of endothelial branches, when the thickness of hepatic microvillus was set to be 0.0 (e), 0.4 (f), or 0.8 μm (g), or when the thickness of endothelium was set to be 0.5 (h), 1.0 (i), or 1.5 μm (j). (k) Shear stress profile at permeability coefficient of endothelial cells of 2.5×10^{-16} m^2.

maximum and averaged FFA concentration difference yield 46.15% and 35.90%, respectively, at the entrance, while they read respective 62.96% and 55.06% at the exit or only 2.55% and 1.66% in the middle segment. It can be seen that highly concentrated FFAs are diffused into the Disse space when the endothelium becomes more permeable [Figs. 4(a)–4(d)]. These results indicated that changes in endothelial permeability can affect FFA metabolism in hepatocytes at the branches. Furthermore, the distribution of FFA concentration is similar to that of flow velocity. At each of the two bifurcation fusion cross sections, FFA concentration presents an approximately bimodal curve along y axis distance [Figs. 4(e) and 4(f)], whereas the profile is likely parabolic at the middle cross section [Fig. 4(g)]. In contrast to the flow velocity profile, however, the FFA profile tends to be concave-distributed, presumably due to the outcomes from FFA chemical reactions with their enzymes. Moreover, shear-forced diffusion is able to enlarge these polarizations, as compared to that from free diffusion. In a single-straight sinusoid, more FFAs are able to diffuse into the Disse space based on FFA reaction–diffusion when the endothelium is more permeable [Figs. 4(h)–4(k)], consistent with those in a dual-branched sinusoid. By contrast,

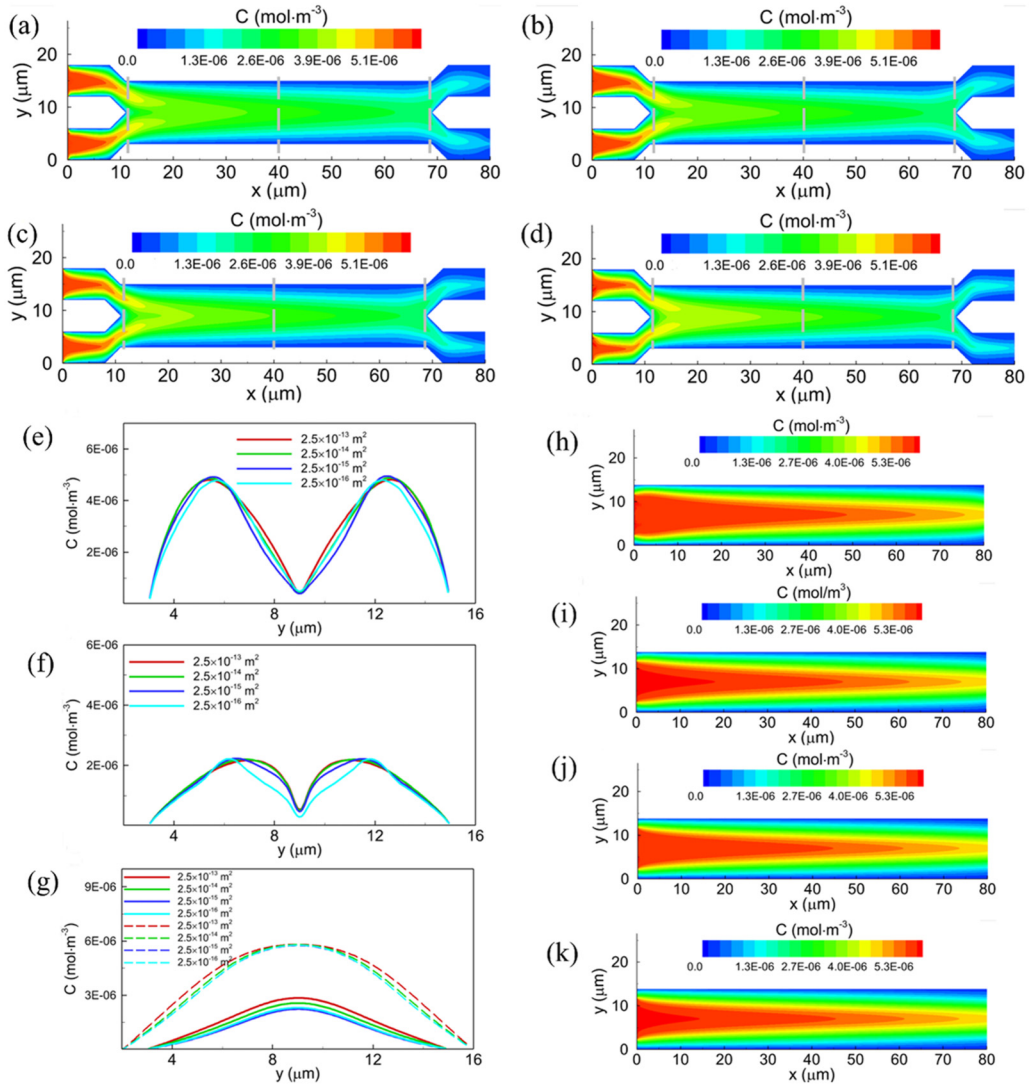

FIG. 4. (a)–(d) FFA concentration distribution in a dual-branched sinusoid at permeability coefficient of the endothelial layer of 10^{-13} (a), 10^{-14} (b), 10^{-15} (c), or 10^{-16} m^2 (d). (e) and (f) FFA concentration profiles at $x = 11$ (e), 69 (f), or 40 μm (g) when $k_{FFA} = 3.0 \times 10^3$ s^{-1}. *Dotted lines* in **g** denoted FFA concentration distribution curve at the middle cross section of the single-channel sinusoid. (h)–(k) FFA concentration distribution in a single-straight sinusoid at permeability coefficient of the endothelial layer of 10^{-13} (h), 10^{-14} (i), 10^{-15} (j), or 10^{-16} m^2 (k).

these maximum and average difference values of FFA concentration are 27.49% and 14.81% in the single-straight sinusoid model. It is worth noting that the average difference between the two models in the middle segment is 56.51%, presenting a considerable difference.

Distribution of the lipoprotein concentration is also calculated in the dual-branched sinusoid after hepatocyte-generated VLDL (Fig. 5). VLDL concentration at the cross sections of the two branches is significantly different with varied endothelial permeability coefficients [Figs. 5(a)–5(d)]. When the endothelial permeability is low, a high VLDL concentration is presented in the Disse space at the branch, where the lipoprotein concentration distribution is evidently polarized [Figs. 5(e) and 5(f)]. This negative correlation between endothelial permeability and VLDL concentration further reduces endothelial permeability, which in turn aggravates lipoprotein polarization. Again, the distribution of lipoprotein concentration is different from that of the flow velocity. Lipoprotein polarization in this confluence segment is obvious, and the VLDL distribution profile exhibits a single peak curve [Figs. 5(e) and 5(f)], whereas the flow velocity is low and exhibits double-peaked curve at this segment [Figs. 2(d) and 2(e)]. Furthermore, VLDL

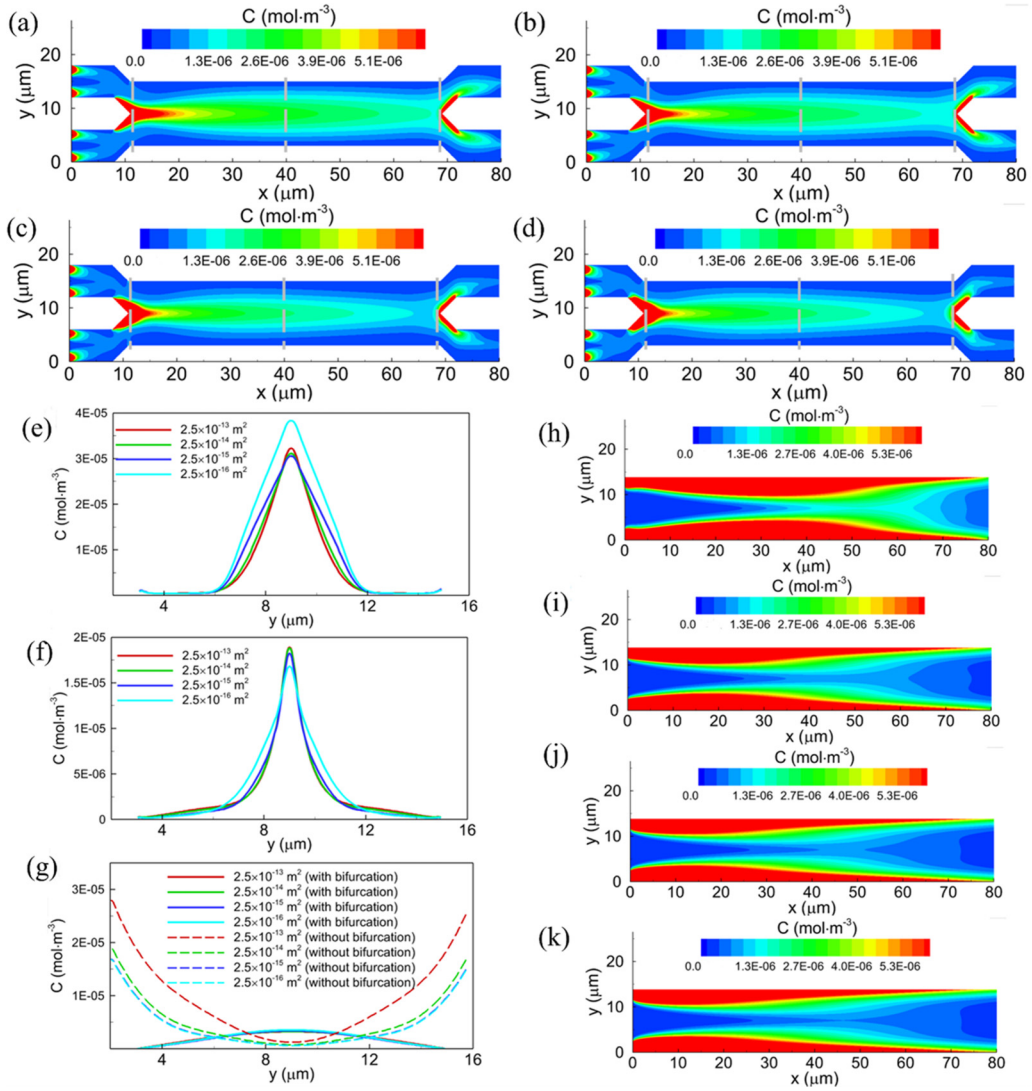

FIG. 5. (a)–(d) VLDL concentration distribution in a dual-branched sinusoid at permeability coefficient of endothelial layer of 10^{-13} (a), 10^{-14} (b), 10^{-15} (c), or 10^{-16} m^2 (d). (e) and (f) VLDL concentration profiles at $x = 11$ (e), 69 (f), or 40 μm (g) when $k_{VLDL} = 3.0 \times 10^3$ s^{-1}. *Dotted lines* in **g** denoted VLDL concentration distribution curve at the middle cross section of the single-channel sinusoid. (*h-k*) VLDL concentration distribution in a single-straight sinusoid at permeability coefficient of the endothelial layer of 10^{-13} (h), 10^{-14} (i), 10^{-15} (j), or 10^{-16} m^2 (k).

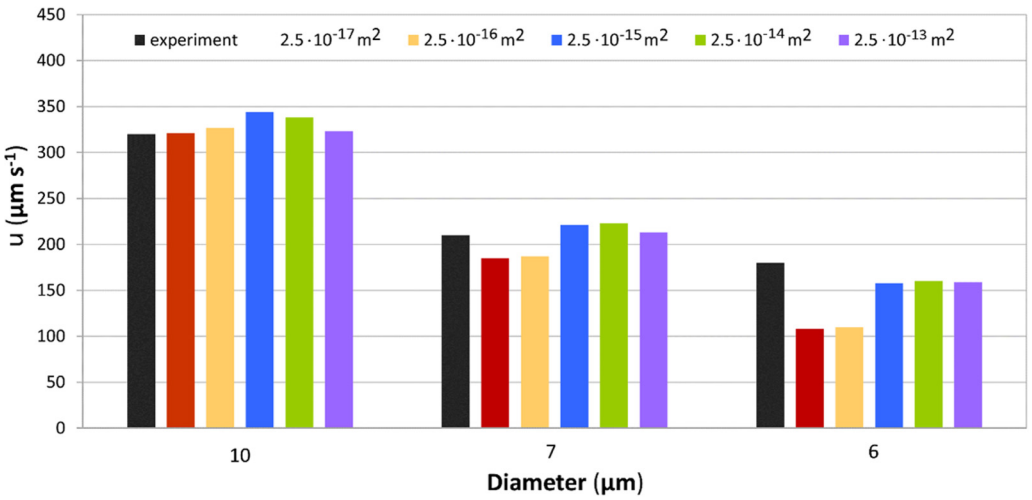

FIG. 6. Comparisons between experimental data[8] and numerical simulations of blood flow velocity in hepatic sinusoid.

concentration distribution was compared between a dual-branched sinusoid and a single-straight sinusoid. In a single-straight sinusoid, the more permeable the endothelium the higher is the VLDL concentration in the sinusoidal cavity based on lipoprotein reaction–diffusion [Figs. 5(h)–5(k)], suggesting that decreasing endothelial permeability increases lipoproteins deposition in the Disse space. Collectively, these results in a single-straight sinusoid are consistent with those for FFA metabolism and lipoprotein deposition at the confluence of a dual-branched sinusoid. Specifically at the branch intersection in a dual-branched sinusoid, the polarized lipoprotein concentration distribution is more prominent when the branches are present.

Furthermore, the flow velocity distribution in a dual-branched hepatic sinusoid is evidently different from that in a single-channel hepatic sinusoid. Due to the influence of the bifurcated structure and the existence of the space of Disse, the velocity in the lumen of a dual-branched sinusoid yields a non-monotonic variation with the endothelial permeability coefficient. This non-monotonic variation of the velocity in the two branches is meaningful to predict hemodynamic alterations in the abnormal liver sinusoids, which is even more complicated and hard to quantify *in vivo*. Future works will focus on comparing the flow features in the straight and branched sinusoids experimentally and numerically in either healthy or fibrotic/cirrhotic livers, in which numerical simulations can provide the bases of mechanistic analysis and data quantification.

Comparison with experimental observations

These numerical simulations were further compared with the experimental measurements of hepatic sinusoidal flow velocity. Hepatic sinusoid blood flow velocity was measured previously in mice with different tube diameters,[25] yielding the value of $320\,\mu m\,s^{-1}$ at a typical $10\,\mu m$ diameter. Assuming the plasma viscosity of 1.2 cp and the Reynolds number is 2.7×10^{-3}, the experimental readouts at 7 and $6\,\mu m$-diameter could be related to those mice under different degrees of fatty liver. Measured data showed that the blood flow velocity also decreased when the tube diameter decreased. Using the fluorescent dye of hepatic sinusoids to observe the obvious overflow, it was indicated that the permeability of hepatic sinusoids increased at this time. The hepatic sinusoid velocity under varied tube diameters and endothelial permeabilities was also calculated using those parameters in Ref. 25, as seen in Fig. 6, where the endothelial permeability was assumed to range from 10^{-17} to $10^{-13}\,m^2$. Here, the blood flow velocity increased first and then decreased with the increased endothelial permeability at 7 and $6\,\mu m$-diameter cases. In particular, when the permeability was greater than $10^{-15}\,m^2$, the blood flow velocity increased significantly. Whereas the permeability coefficient is sufficiently small ($<10^{-15}$), the change of the blood flow from the space of Disse into the sinusoidal lumen with the permeability coefficient is evident. When the permeability coefficient increases, the flow into the sinusoidal lumen is less varied due to the high permeability at this time. Furthermore, as the diameter was reduced to $6\,\mu m$, which is quite small, the velocity changed slightly with the endothelial permeability. In other words, the blood flow velocity decreases with the decrease of tube diameter, and the blood flow velocity increases with the increase of the permeability in fatty liver mice. These simulations are consistent with the experimental measurements, and the comparisons between numerical calculations and measured data, specifically for average blood flow velocity in the sinusoidal lumen, yielded a minimum error of 2.2% ($10\,\mu m$) and a maximum error of less than 37% ($6\,\mu m$). The errors were presumably attributed to the parameter sensitivity, which could not be quantified directly by the experimental approach yet. The results validated the rationality and accuracy of the proposed model.

DISCUSSION

This work aimed at clarifying the differential flow dynamics and mass transportation between a dual-branched and a single-straight

liver sinusoid. Results indicated that the flow velocity of single-channel hepatic sinusoids increased with the increase of the permeability coefficient of the endothelial cell layer, showing a monotonic transition. While the flow velocity of the dual-branched hepatic sinusoids showed a non-monotonic transition with the permeability of the endothelial cell layer due to the influence of bifurcation structure. Meanwhile, regardless of the single-channel model or the dual-branch model, flow-induced shear stress on the endothelium at the side of the Disse space exhibited a biphasic pattern, that is, when the permeability coefficient of the endothelium is large or small, the flow-induced shear stress has an opposite change with reduced or enhanced value with the increase of the thickness of the endothelium. This biphasic pattern is likely caused by the small size of the Disse space and the permeability of endothelium, and the bifurcation structure has no effect on the biphasic pattern. Evidently, the effect of endothelial permeability on the flow-induced shear stress in the single-channel model is different from those in the dual-branched model. Our previous work[30] showed that the shear stress of single-channel decreased with the decrease of endothelial permeability when the thickness of the endothelial cell layer was constant. However, when the thickness of the endothelial cell layer remained unchanged in the dual-branched model, the shear stress first decreased and then increased with the decrease of endothelial permeability, which was related to the non-monotonic transition of blood flow velocity in the dual-branched model. It should be noted that the hepatic sinusoid model in this work yields a branched structure. As the blood flows through this branched region of the hepatic sinusoid, it experiences abrupt changes in geometry, which may highlight the non-Newtonian fluid effects of the blood.

In this work, the substance concentration distributions under varied endothelial permeability coefficient and substance diffusion coefficient are also different. For example, when the endothelial permeability coefficients decrease from 10^{-13} to 10^{-16} m2 at the intersection position in a dual-branched sinusoidal model, the FFA and VLDL concentrations are increased by 13.9% and 21.0%, respectively. However, when the endothelial permeability coefficient is decreased from 10^{-13} to 10^{-16} m2 in a single-straight sinusoid, the VLDL concentration is decreased by 51.1% (at the position of $x = 40\,\mu$m, $y = 7\,\mu$m) and the FFA concentration is decreased only 0.9% at the same position. That is, these variations may depend on those permeability and diffusion coefficients. Future validation is required using robust experimental data.

Flow-accompanied mass transport is also crucial in the progress of liver fibrosis and cirrhosis. Thus, the similarities and differences of FFA and VLDL material transport in single-channel and dual-branch models were further tested. Figure 4(g) showed the comparisons of fatty acid concentration distributions in the middle segment of the dual-branched model and the single-channel model. Results showed that, regardless of the single-channel or dual-branched model, the concentration of fatty acid in the lumen of the blood sinusoid was higher. As seen in Fig. 5(g), the distribution of lipoprotein concentration in the middle segment in the dual-branched model was significantly different from that in the single-channel hepatic sinus model. The lipoprotein concentration in the upper and lower sides of the single channel was higher than that in the sinusoid of the dual-branched model, mainly because the concentration of lipids entering the Disse space in the single channel is higher than in the dual-branched model and more lipoproteins are formed in the Disse space. In addition, lipoprotein concentration in the confluence segment of the dual-branched model came from the Disse space at the junction of branches and was even higher in the Disse space, thus promoting the increase of lipoprotein concentration in the sinusoid. In conclusion, the branched structure of hepatic sinusoids can also cause the difference in the distributions of biochemical materials concentration in hepatic sinusoids.

In addition, the process of liver cells metabolizing blood ammonia into urea has also been simulated in a single channel by assuming that blood ammonia flows in from the left side and flows out from the right side.[27] At the bottom of the channel is the layer of liver cells, which metabolize the blood ammonia flowing through the channel into urea. After the metabolism of liver cells, the distribution of serum ammonia concentration in a single channel is characterized as follows: altering from low to high concentration from the bottom to the top side and from high to low concentration approximately linearly from the left and right side. Thus, the FFA concentration distribution in this work is similar to their simulations,[27] in the way that it changes linearly from high to low concentration along the length of the passage from the left to the right side. In that work, blood ammonia flows in from the left inlet, and its concentration gradually decreases at the outlet due to the continuous metabolic consumption of hepatocytes, which is consistent with the simulations in this work [Figs. 4(h)–4(k)]. Different from the simulation results in this literature,[27] our simulations for FFA concentration alter from low to high and then to low concentration again, presumably due to the existence of the top layer of liver cells in our model, resulting in the concentration decrease from bottom to the top side followed by the concentration increase. Future liver chip-based tests are required to validate these predictions.

CONCLUSIONS

When the liver is in a pathological state, such as fatty liver or liver fibrosis or cirrhosis, the hemodynamics of hepatic sinusoids is different from that of the normal liver due to the deposition of lipid, collagen, and other substances, as well as due to the capillary vascularization of endothelial cells. These pathophysiological outcomes of hepatic sinusoids are quite complicated, thus rendering the difficulty to obtain blood flow details using direct experimental measurements. Therefore, the LBM was used here to establish the dual-branch hepatic sinusoidal blood flow model, and the effects of endothelial permeability, endothelium thickness, hepatic microvillus, and collagen layer on the flow velocity and cell surface blood shear stress were discussed. Results show that the flow velocity in the sinusoidal cavity with confluent branches demonstrates a non-monotonic change with endothelial permeability. This non-monotonic variation of the velocity in the two branches is meaningful to predict hemodynamic alterations in the abnormal liver sinusoids, which is even more complicated and hard to quantify *in vivo*. The shear stress of blood flow in the Disse space of endothelial cells had a biphasic pattern due to the influence of microflow. The flow velocity distribution in a double-branched hepatic sinusoid is evidently different from that in a single-channel hepatic sinusoid. Meanwhile, a highly polarized distribution of lipoproteins

concentration was also observed at the low shear stress region, indicating a localized accumulation of typical hepatic serum proteins. Finally, the experimental and numerical results of intrahepatic flow velocity in mice with fatty liver were compared, in accordance with that the diameter of hepatic sinusoids decreased, the flow velocity decreased, and the tortuosity and permeability of hepatic sinusoids increased in mice with fatty liver. Thus, our simulations furthered the understanding in the relationship between the changes in blood flow in hepatic sinusoids and the related liver lesions. Future works will focus on comparing the flow features in straight and branched sinusoids experimentally and numerically in either healthy or fibrotic/cirrhotic livers, in which numerical simulations can provide the bases of mechanistic analysis and data quantification.

ACKNOWLEDGMENTS

The authors are grateful for Dr. Tianhao Wang, Dr. Shenbao Chen, Dr. Luwen Zhou, and Dr. Shiliang Feng for technical assistance and helpful discussions. This work was supported by the National Natural Science Foundation of China (NNSFC) (Grant No. 11972252), the Frontier Science Key Project of Chinese Science Academy (Grant No. QYZDJ-SSW-JSC018), and the Tianjin Natural Science Foundation (Grant No. 17JCYBJC29300).

AUTHOR DECLARATIONS

Conflict of Interest

The authors declare no competing interests.

Author Contributions

S.L., Y.C., and M.L. designed the study. Y.H. and Y.C. developed analytical theory and completed the simulation. W.L. analyzed the data. Y.H. and Y.C. wrote the manuscript. S.L. and M.L. edited the manuscript and approved the final draft.

Yinjing Hao: Data curation (equal); Formal analysis (equal); Methodology (equal); Software (equal); Writing – review & editing (equal). **Shouqin Lü:** Conceptualization (equal); Data curation (equal); Supervision (equal); Writing – review & editing (equal). **Wang Li:** Formal analysis (equal); Methodology (equal). **Mian Long:** Methodology (equal); Validation (equal); Writing – review & editing (equal). **Yuhong Cui:** Methodology (equal); Supervision (equal); Validation (equal); Writing – review & editing (equal).

DATA AVAILABILITY

The data that support the findings of this work are available from the corresponding authors upon reasonable request.

REFERENCES

[1]X. Shu, N. Li, Y. Wu, W. Li, X. Zhang, P. Li, D. Lü, S. Lü, and M. Long, Acta Mech. Sin. **37**, 201 (2021).
[2]Q. Zhang, J. Yu, T. Guo, L. Tian, J. Quan, W. Lin, X. E. Niu, and J. Liu, "High glucose/ox-LDL induced hepatic sinusoidal capillarization via αvβ5/FAK/ERK signaling pathway," Biochem. Biophys. Res. Commun. **513**, 1055 (2019).
[3]H. Adel, "P. R. Role of liver sinusoidal endothelial cells in non-alcoholic fatty liver disease," J. Hepatol. **70**, 1278 (2019).
[4]L. An, X. Li, Y. Liu, X. Liu, and X. Chu, J. Exp. Hematol. **28**, 242 (2020).
[5]L. Li and Y. Liu, J. Clin. Hepatol. **35**, 913 (2019).
[6]W. Lin, Ph.D. thesis, Lanzhou University, 2019.
[7]B. Ma, X. Han, D. Shi, and G. Ying-Hui, J. Med. Imaging **18**, 1133 (2008).
[8]L. Yang, L. Ma, and Y. Luo, J. Sichuan Univ. **47**, 326 (2016).
[9]R. M. Amir, M. D. Khadijeh Bakhtavar, M. D. Nasser Ebrahimi-Daryani, P. Habibollahi, and S. Abdollahzade, J. Clin. Ultrasound. **7**, 346 (2010).
[10]S. Ehsan, M. Fariborz, M. Roghaeyh, and J. Farahnaz, Hepat. Mon. **9**, 740 (2011).
[11]J. Hu, S. Lü, S. Feng, and M. Long, Acta Mech. Sin. **33**, 823 (2017).
[12]S. Jeon and R. Carr, J. Lipid Res. **61**, R119000547 (2020).
[13]R. A. Sinha, B. K. Singh, and P. M. Yen, Nat. Rev. Endocrinol. **14**, 259 (2018).
[14]H. Zhou and R. Liu, Front Genet. **5**, 112 (2014).
[15]X. Wang, Contin. Med. Educ. China **11**, 157 (2019).
[16]K. F. Leavens and M. J. Birnbaum, Crit. Rev. Biochem. Mol. Biol. **46**, 200 (2011).
[17]W. Han, S. Liu, Z. Duan, and W. U. Qiao, Chin. J. Gastroenterol. Hepatol. **27**, 1103 (2018).
[18]D. B. Jump, Curr. Opin. Clin. Nutr. Metab. Care **14**, 115 (2011).
[19]R. Nosadini, A. Avogaro, and G. Crepaldi, J. Clin. Endocrinol. Metab. **58**, 1125 (1984).
[20]V. D. Graaff, W. J. Kwanten, and S. M. Francque, Med. Hypotheses **122**, 188 (2019).
[21]Z. Wang and B. Wang, Chin. J. Integr. Traditional Western Med. Imaging **13**, 458 (2015).
[22]P. Chen, X. Cheng, and Y. Guo, Jilin Med. Sci. **40**, 1184 (2019).
[23]X. Hang and J. Zhu, Imaging Res. Med. Appl. **2**, 44 (2018).
[24]C. Chen, J. Fan, and W. Zhang, J Anat. **50**, 645 (2019).
[25]J. Fan, C. J. Chen, Y. C. Wang, W. Quan, J. W. Wang, and W. G. Zhang, World J. Gastroenterol. **25**, 1355 (2019).
[26]Y. Li, Y. Liu, and J. Zhang, World J. Integr. Chin. Western Med. **9**, 607 (2014).
[27]H. P. Rani, T. W. H. Sheu, T. M. Chang, and P. C. Liang, J. Biomech. **39**, 551 (2006).
[28]F. Sharifi, B. Firoozabadi, M. S. Saidi, and K. Firoozbakhsh, in *Iranian Research Organization for Science and Technology* (IEEE, Piscataway, NJ, 2015), Vol. 25.
[29]Z. Z. Shi, K. Stephen, B. A. David, and C. Wu, Plos One **1**, 1–39 (2016).
[30]T. H. Wang, S. Lu, Y. Hao, Z. Su, M. Long, and Y. Cui, Biophys. J. **120**, 4859 (2021).
[31]T. W. Secomb, R. Hsu, and A. R. Pries, Microcirculation **9**, 189 (2002).
[32]C. Kleinstreuer and J. Koo, J. Fluids Eng. **126**, 1 (2004).
[33]Y. Du, N. Li, H. Yang, C. Luo, Y. Gong, C. Tong, Y. Gao, S. Lu, and M. Long, Lab Chip **17**, 782 (2017).
[34]G. Pan, G. Ding, and C. Dai, China Elastomerics **22**, 29 (2012).